Propagation and localization of electromagnetic waves in quasiperiodic serial loop structures

H. Aynaou,[1] E. H. El Boudouti,[1] Y. El Hassouani,[1] A. Akjouj,[2,*] B. Djafari-Rouhani,[2] J. Vasseur,[2] A. Benomar,[2] and V. R. Velasco[3]

[1]*Laboratoire de Dynamique et d'Optique des Matériaux, Département de Physique, Faculté des Sciences, Université Mohamed Premier, 60000 Oujda, Morocco*

[2]*Laboratoire de Dynamique et Structure des Matériaux Moléculaires, UMR CNRS 8024, UFR de Physique, Université de Lille 1, F-59655 Villeneuve d'Ascq, France*

[3]*Instituto de Ciencia de Materiales de Madrid, CSIC, Sor Juana Inés de la Cruz 3, 28049 Madrid, Spain*

(Received 14 March 2005; revised manuscript received 9 August 2005; published 3 November 2005)

We study the propagation of electromagnetic waves in one-dimensional quasiperiodic photonic band gap structures made of serial loop structures separated by segments. Different quasiperiodic structures such as Fibonacci, Thue-Morse, Rudin-Shapiro, and double period are investigated with special focus on the Fibonacci structure. Depending on the lengths of the two arms constituting the loops, one can distinguish two particular cases. (i) There are symmetric loop structures, which are shown to be equivalent to impedance-modulated mediums. In this case, it is found that besides the existence of extended and forbidden modes, some narrow frequency bands appear as defect modes in the transmission spectrum inside the gaps. These modes are shown to be localized within only one of the two types of blocks constituting the structure. An analysis of the transmission phase time enables us to derive the group velocity as well as the density of states in these structures. In particular, the stop bands (localized modes) may give rise to unusual (strong normal) dispersion in the gaps, yielding fast (slow) group velocities above (below) the velocity of light. (ii) There are also asymmetric loop structures, where the loops play the role of resonators that may introduce transmission zeros and hence additional gaps unnoticed in the case of simple impedance-modulated mediums. A comparison of the transmission amplitude and phase time of Fibonacci systems with those of other quasiperiodic systems is also outlined. In particular, it was shown that these structures present similar behaviors in the transmission spectra inside the regions of extended modes, whereas they present different localized modes inside the gaps. Experiments and numerical calculations are in very good agreement.

DOI: 10.1103/PhysRevE.72.056601 PACS number(s): 41.20.Jb, 77.84.Lf

I. INTRODUCTION

The study of elementary excitations in multilayered structures with constituents arranged in quasiperiodic sequences has been an active field of research during the last decade [1]. Among them, optical waves in quasiperiodic photonic crystals have received a great deal of attention so as to show the localization of light incident on dielectric multilayers [2–14]. These structures have been proposed to design optical microcavities [15] and omnidirectional reflectors [16] of practical interest. Recently, it was shown [7] experimentally that Fibonacci and aperiodic dielectric multilayers with internal symmetry may have potential applications in multiwavelength narrow band optical filters and wavelength division multiplexing systems. Also, it was demonstrated [8] that these systems can provide an interesting alternative to regular photonic crystals for the realization of photonic devices, such as optical filters with a self-similar spectrum and a high wavelength selectivity in the band edge region. Because of their noninteracting nature, electromagnetic waves provide an excellent tool for probing the localization phenomena [3,4] in comparison with other excitations such as electronic waves. Until now, as far as we know, mainly electromagnetic wave propagation in one-dimensional (1D) quasiperiodic systems has been studied in 1D Fibonacci lossless multilayered media [3–8].

In the present paper, we consider a different quasiperiodic photonic crystal made of segments and loops (Fig. 1), called a Fibonacci loop structure (FLS). Such a structure may present similar results to those of layered media for symmetrical loops. However, the results are quite different for asymmetrical loops as the latter may introduce transmission

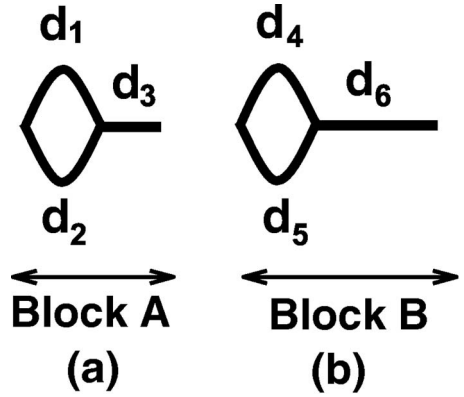

FIG. 1. (a) and (b) Schematic illustrations of the A and B blocks from which the Fibonacci structure is composed. Each block A (B) is constructed from a loop of length d_1+d_2 (d_4+d_5) connected to a segment of length d_3 (d_6).

*Corresponding author. Electronic address: Abdellatif.Akjouj@univ-lille1.fr

zeros and hence new gaps in the transmission spectrum unnoticed in layered media. Also, when the media constituting the FLS are made of standard coaxial cables of the order of 1 m with small cross sections, the propagation becomes monomode and one can obtain very accurate experimental results that may be fitted with a simple 1D theoretical model. In two recent papers [17,18], we have presented these results in the case of periodic loop structures (PLSs) made of coaxial cables. In particular, we have shown that these structures may present large stop bands and are good candidates for photonic band gap (PBG) materials [19]. In addition, measurements of the amplitude and the phase of the transmission enabled us to deduce several properties of the wave propagation through such structures, such as dispersion curves, phase times, or equivalently density of states, as well as group velocities. We have also shown that the introduction of a single defect in the PLS gives rise to well-defined defect modes inside the band gaps in the transmission spectra. Based on the above knowledge in periodic loop structures, the object of this paper is to put emphasis on similar phenomena in quasiperiodic loop structures which have not been investigated before. The results are also compared with those of the periodic structures obtained before. In particular, we show that besides to extended modes that characterize periodic structures, quasiperiodic systems may exhibit new modes showing self-similarities in the amplitude and the phase of the transmission spectrum. These modes are related to the quasiperiodicity of the system and are without analog in periodic systems.

In a recent work [20], Zhang *et al.* studied theoretically and experimentally three-dimensional PBG systems formed by segments and symmetrical loops made of coaxial cables arranged in a diamond structure. In addition to the Anderson localized state observed in random structures, defect modes are introduced in the gap by changing the length of one loop in an ordered network. However, the peak associated with the defect mode is not well defined because of the dissipation in the cables. In this article, we show that a 1D structure made of segments and loops may clearly show the origin of the band gap of Fibonacci structures as a function of the different lengths of segments and loops. In addition, we show that in addition to the transmission amplitude, an analysis of the transmission phase time enables us to determine the density of states as well as the group velocities in these structures. The quasiperiodic structures are generally formed as substitutional sequences built of two different building blocks A and B. One of the well-known examples is the Fibonacci sequence $S_{j+1}=S_jS_{j-1}$ with the initial conditions $S_1=A$, $S_2=AB$, where j is the generation number. For example $S_3=ABA$, $S_4=ABAAB$, $S_5=ABAABABA$,... and the number of building blocks A and B in the infinite order sequence is equal to the golden mean number $\tau=(1+\sqrt{5})/2$ for large j. In this work, we consider that the block A (B) is constructed of a loop of length d_1+d_2 (d_4+d_5) connected to a segment of length d_3 (d_6) (all the six lengths are considered to be different from each other; see Fig. 1). Let us notice that some preliminary results of this work are presented elsewhere [21].

The theoretical system developed here falls within the framework of the Green's function method, which we recall briefly in Sec. II. Section III is devoted to a numerical discussion of the theoretical results and the comparison to the experimental measurements of the electromagnetic transmission spectra through a finite FLS composed of standard coaxial cables. A comparison of the Fibonacci transmission amplitude and phase time with those obtained in other quasiperiodic structures is illustrated in Sec. IV. Finally some conclusions are drawn in Sec. V.

II. METHOD OF THEORETICAL AND NUMERICAL CALCULATION

A. Interface response theory of continuous media

Our theoretical analysis is performed with the help of the interface response theory of continuous media [22], which allows calculating the Green's function of any composite material. In what follows, we present the basic concept and the fundamental equations of this theory [22]. Let us consider any composite material contained in its space of definition D and formed out of N different homogeneous pieces located in their domains D_i. Each piece is bounded by an interface M_i, adjacent in general to j $(1 \leqslant j \leqslant J)$ other pieces through subinterface domains M_{ij}. The ensemble of all these interface spaces M_i will be called the interface space M of the composite material. The elements of the Green's function $g(DD)$ of any composite material can be obtained from [22]

$$g(DD) = G(DD) - G(DM)G^{-1}(MM)G(MD) + G(DM)G^{-1}(MM)g(MM)G^{-1}(MM)G(MD), \tag{1}$$

where $G(DD)$ is the reference Green's function formed out of truncated pieces in D_i of the bulk Green's functions of the infinite continuous media and $g(MM)$ is the interface element of the Green's function of the composite system. The inverse of $g(MM)$ is obtained as a superposition of the different $[g_i(M_i,M_i)]^{-1}$, where $g_i(M_i,M_i)$ is the interface Green's function for each constituent i of the composite system [22]. Knowledge of the inverse of $g(MM)$ is sufficient to calculate the interface states of a composite system through the relation [22]

$$\det[g^{-1}(MM)] = 0. \tag{2}$$

Moreover if $U(D)$ represents an eigenvector of the reference system, Eq. (1) enables the calculation of the eigenvectors $u(D)$ of the composite material and

$$u(D) = U(D) - U(M)G^{-1}(MM)G(MD) + U(M)G^{-1}(MM)g(MM)G^{-1}(MM)G(MD). \tag{3}$$

In Eq. (3), $U(D)$, $U(M)$, and $u(D)$ are row vectors. Equation (3) provides a description of all the waves reflected and transmitted by the interfaces, as well as the reflection and transmission coefficients of the composite system. ln this case, $U(D)$ is a bulk wave launched in one homogeneous piece of the composite material [23].

B. Inverse surface Green's functions of the elementary constituents

We consider an infinite homogeneous isotropic dielectric wire i characterized by its characteristic impedance Z_i. The Fourier transformed Green's function between two points x and x' of this wire is

$$G_i(x,x') = \frac{jZ_i}{2} e^{-\alpha_i |x-x'|}, \tag{4}$$

with

$$\alpha_i = -j\frac{\omega}{c}\sqrt{\varepsilon_i}, \tag{5}$$

where ε_i is the relative permittivity, ω the angular frequency of the wave, c the speed of light in vacuum, and $j=\sqrt{-1}$.

Before addressing the problem of a FLS, it is helpful to know the surface elements of its elementary constituents, namely, the Green's function of a finite segment of length d_i, of a loop (k,l) made of two wires k and l of lengths d_k and d_l, respectively, and of a semi-infinite wire s. The finite segment is bounded by two free surfaces located at $x=-d_i/2$ and $x=+d_i/2$. These surface elements can be written in the form of a (2×2) matrix $g_i(MM)$, within the interface space $M_i=\{-d_i/2,+d_i/2\}$. The inverse of this matrix takes the following form [23]:

$$[g_i(MM)]^{-1} = \begin{pmatrix} \frac{C_i}{Z_i S_i} & -\frac{1}{Z_i S_i} \\ -\frac{1}{Z_i S_i} & \frac{C_i}{Z_i S_i} \end{pmatrix}, \tag{6}$$

for the segments $i=3$ in the block A and $i=6$ in the block B (Fig. 1).

In the same way, the inverse of the Green's function of the loop (k,l) is obtained as [23]

$$[g_{k,l}(MM)]^{-1} = \begin{pmatrix} \frac{C_k}{Z_k S_k} + \frac{C_l}{Z_l S_l} & -\frac{1}{Z_k S_k} - \frac{1}{Z_l S_l} \\ -\frac{1}{Z_k S_k} - \frac{1}{Z_l S_l} & \frac{C_k}{Z_k S_k} + \frac{C_l}{Z_l S_l} \end{pmatrix}, \tag{7}$$

where $(k,l)=(1,2)$ in the block A and (4,5) in the block B (Fig. 1). $C_i=\cos[(\omega/c)\sqrt{\varepsilon_i}d_i]$ and $S_i=\sin[(\omega/c)\sqrt{\varepsilon_i}d_i]$ in Eqs. (6) and (7). The inverse of the surface element of a semi-infinite waveguide s characterized by its impedance Z_s is given by

$$[g_s(0,0)]^{-1} = -\frac{j}{Z_s}. \tag{8}$$

From Eq. (7) one can deduce that a symmetric loop made of identical wires of lengths $d_k=d_l$ and impedances $Z_k=Z_l$ is equivalent to a single segment of length d_k and characterized by the impedance $Z_k/2$. Therefore, each block (Fig. 1) becomes equivalent to two different segments connected together (bisegment). Experimental evidence of the existence of band gaps and defect modes in 1D periodic photonic systems constructed by two alternative coaxial cables of different characteristic impedances was presented recently [24,25]. However, the advantage of the symmetric loop structure lies in the fact that it is not necessary to have two segments of different nature to realize the contrast between the two constituent media of each block. This property could be of potential interest in optical waveguide structures.

C. Transmission coefficient

The 1D FLS waveguide can be considered as a finite number of blocks A and B pasted together according to the Fibonacci sequence. The interface domain is made of all the connection points between finite segments and loops. Within the total interface space of the finite FLS, the inverse of the matrix giving all the interface elements of the Green's function g is a finite tridiagonal matrix formed by linear superposition of the elements $[g_i(MM)]^{-1}$ [Eqs. (6) and (7)]. The explicit expression of the Green's function elements of the finite FLS may be written as

$$g_f^{-1}(MM) = \begin{pmatrix} g_f^{-1}(\ell,\ell) & g_f^{-1}(\ell,r) \\ g_f^{-1}(r,\ell) & g_f^{-1}(r,r) \end{pmatrix} \tag{9}$$

where the labels ℓ (left) and r (right) refer to the two interfaces bounding the FLS. The four matrix elements are real quantities, functions of the different elements of the constituent's elements $g_i(MM)$ [Eqs. (6) and (7)]. If the finite composite system is connected on both sides to two homogeneous waveguides labeled s, then an incident plane wave launched from the left waveguide gives rise to the transmission function in the right waveguide as

$$C_T = \frac{-2jg_f^{-1}(l,r)/Z_s}{g_f^{-1}(\ell,\ell)g_f^{-1}(r,r) - [g_f^{-1}(l,r)]^2 - (1/Z_s)^2 - j[g_f^{-1}(\ell,\ell) + g_f^{-1}(r,r)]/Z_s}. \tag{10}$$

The transmission function can be written in an explicit complex form as $C_T=a+jb=\sqrt{T}e^{j\varphi}$ where T is the transmission coefficient, $\varphi=\arctan(b/a)\pm m\pi$ is the phase associated with the transmission field, and m is an integer. The first derivative of φ with respect to the frequency is related to the delay time taken by the wave to traverse the structure. This quantity, called phase time, is defined by [26,27]

$$\tau_\varphi = \frac{d\varphi}{d\omega}. \tag{11}$$

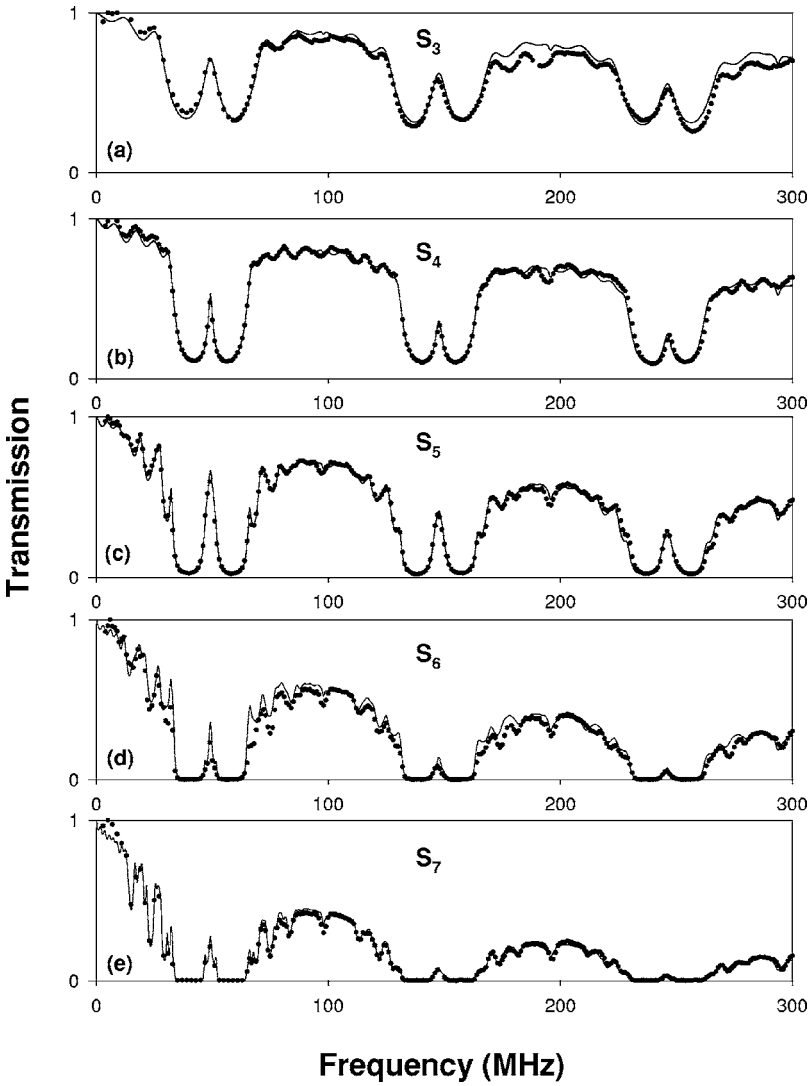

FIG. 2. Theoretical (solid curves) and experimental (dotted curves) variations of the transmission coefficient as a function of the frequency for different generations S_j ($j=3-7$) of the Fibonacci loop structure. The lengths of the different coaxial cables are $d_1=d_2=d_3=d_4=d_5=1$ m, $d_6=2$ m.

From Eqs. (10) and (11), one can deduce that the phase time can be written as

$$\tau_\varphi = \frac{d}{d\omega}\arg\{g_f^{-1}(\ell,\ell)g_f^{-1}(r,r) - [g_f^{-1}(\ell,r)]^2 - (1/Z_s)^2 - j[g_f^{-1}(\ell,\ell) + g_f^{-1}(r,r)]/Z_s\}^{-1} + \frac{d}{d\omega}\arg[g_f^{-1}(\ell,r)]. \tag{12}$$

Furthermore, the density of states (DOS) of the present composite system from which we have subtracted the DOS of the same volumes of the semi-infinite waveguides s is given by [22,27]

$$\Delta n(\omega) = \frac{1}{\pi}\frac{d}{d\omega}\arg\{g_f^{-1}(\ell,\ell)g_f^{-1}(r,r) - [g_f^{-1}(\ell,r)]^2 - (1/Z_s)^2 - j[g_f^{-1}(\ell,\ell) + g_f^{-1}(r,r)]/Z_s\}^{-1}. \tag{13}$$

From Eqs. (12) and (13) one can deduce two cases, as follows.

(i) The case of symmetrical loop structures that do not present transmission zeros [i.e., $g_f^{-1}(\ell,r)\neq 0$ in Eq. (10)]. Then $\arg[g_f^{-1}(\ell,r)]=0$ and $\tau_\varphi=\pi\Delta_n(\omega)$.

(ii) The case of asymmetrical loop structures, where transmission zeros occur at some frequencies we denote by ω_n [i.e., $g_f^{-1}(\ell,r)=0$ in Eq. (10), $n=1,2,\ldots$]. Then the transmission coefficient changes sign at ω_n and its phase exhibits a jump of π. In other words, the second term at the right-hand side of Eq. (12) becomes [28]

$$\frac{d}{d\omega}\arg[g_f^{-1}(\ell,r)] = \pi\sum_n \operatorname{sgn}\left(\frac{d}{d\omega}[g_f^{-1}(\ell,r)]_{\omega=\omega_n}\right)\delta(\omega-\omega_n) \tag{14}$$

where sgn means the sign function. This result means that $\tau_\varphi \neq \pi\Delta_n(\omega)$ as τ_φ [Eq. (12)] may exhibit δ functions at the transmission zeros that do not exist in the variation of the DOS [Eq. (13)]. Both of these cases (i) and (ii) will be illustrated below in relation to symmetric and asymmetric FLSs, respectively.

III. NUMERICAL AND EXPERIMENTAL RESULTS

For the sake of simplicity, we have limited ourselves to the case of media constituting a FLS made of standard coaxial cables [i.e., $Z_i=Z=50\ \Omega$ and $\varepsilon_i=\varepsilon=2.3$ $(i=1,2,\ldots,6)$]. Also in order to understand the effect of segments and loops in the FLS, we shall emphasize two particular cases.

(1) The case where the loops in each block are symmetrical and identical (i.e., $d_1=d_2=d_4=d_5=d=1$ m) while the segments are supposed to be different (we labeled $d_3=d_A$ in the block A and $d_6=d_B$ in the block B) (see Fig. 1). This structure is equivalent to the one studied in Ref. [29] where each block is composed of a bilayer (see also Sec. II B).

(2) The case where the segments are considered to be identical (i.e., $d_3=d_6=d=1$ m) whereas the loops are supposed to be different. We have kept a symmetrical loop in the A block (i.e., $d_1=d_2=d=1$ m) and chosen an asymmetrical loop in the B block (i.e., $d_4\neq d_5\neq 1$ m, without changing the total length of the loop $d_4+d_5=2$ m) (see Fig. 1).

A. Case of symmetrical and identical loops in A and B blocks

As mentioned in Sec. II B, the symmetrical loops in A and B blocks are equivalent to segments of the same length $d=1$ m but with half impedance $Z/2=25\ \Omega$, while the segments in A and B blocks have different lengths, $d_A=1$ m in block A and $d_B=2$ m in block B, and are characterized by the same impedance $Z=50\ \Omega$. Figures 2(a)–2(e) show the transmission coefficient for the generations S_3 (three blocks), S_4 (five blocks), S_5 (eight blocks), S_6 (13 blocks), and S_7 (21 blocks), respectively. The solid curves represent the theoretical results whereas the dotted curves correspond to the experimental ones. The experiments were performed using standard coaxial cables assembled together with metallic T-shaped connectors. The cross section of the cables being negligible compared to their length and to the propagation wavelength, the assumption of monomode propagation is then satisfied. The transmission measurements have been realized by using the tracking generator coupled to a spectrum analyzer in the frequency range of 10–300 MHz. The attenuation inside the coaxial cables was simulated by introducing a complex relative dielectric permittivity $(\varepsilon=\varepsilon'-j\varepsilon'')$. The attenuation coefficient α'' can be expressed as $\alpha''=\varepsilon''\omega/c$. On the other hand, the attenuation specification data supplied by the manufacturer of the coaxial cables in the frequency range of 10–300 MHz can be approximately fitted with the expression $\ln(\alpha'')=a+b\ln(\omega)$, where a and b are two constants. From this fitting procedure, a useful expression for ε'' as a function of frequency can be obtained under the form $\varepsilon''=0.017f^{-0.5}$ where the frequency f is expressed in hertz. The experimental results are very well fitted by the 1D model using the Green's function method. One can notice in Fig. 2 that for a given generation the attenuation inside the cables induces transmission depletion especially at high frequencies. Two regions of frequencies may be distinguished in Figs. 2(a)–2(e): the regions where the transmission falls down rapidly to zero as the generation number increases [these regions correspond to the forbidden modes (gaps)] and the regions where the transmission is more noticeable around

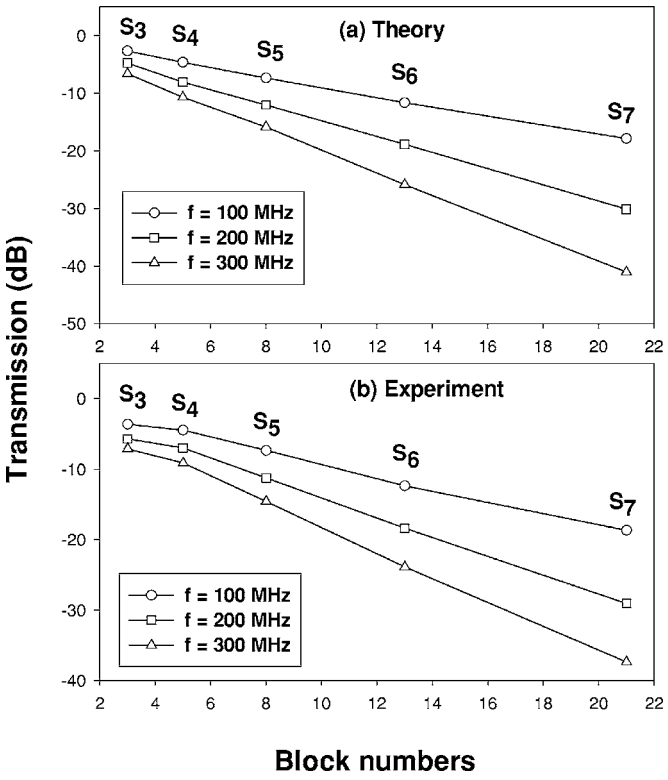

FIG. 3. Theoretical (a) and experimental (b) variations of the transmission coefficient versus the number of blocks in each generation for three frequencies 100, 200, and 300 MHz lying inside the middle of the bulk bands of Fig. 2.

0, 100, 200, and 300 MHz [these regions correspond to the allowed modes (bands)]. In the middle of the gaps around 50, 150, and 250 MHz appear some peaks as defect modes. The frequencies of these modes are independent of the generation number, whereas their intensities increase as function of the generation number, presenting a maximum value at the fifth generation and then decreasing for higher generations. It is worth noticing that in the absence of absorption, this maximum occurs for the fifth and eighth generations as well as for higher generations with a step of order 6 (i.e., the 11th and 14th generations respectively). On the other hand, the transmission inside the bands decreases as the generation number increases as can be seen in Fig. 3 where we have plotted the transmission versus the block numbers for three frequencies 100, 200, and 300 MHz lying in the middle of the bands. The transmission decreases exponentially as a function of the number of blocks in each generation and falls down to zero (−30 dB) beyond the tenth generation. This effect is due to the absorption inside the cables [30] which limits the study of high generation structures.

In order to understand the spatial localization of the different modes in Fig. 2, we plotted in Fig. 4 the calculated local density of states (LDOS) as a function of the space position x for two frequencies 50 and 80 MHz belonging, respectively, to defect modes and bulk bands of Fig. 2(c) (fifth generation). The LDOS reflects the square modulus of the electric field inside the structure. As expected, the mode lying inside the band $(f=80$ MHz) shows a propagating character (extended mode) in the whole structure [Fig. 4(b)],

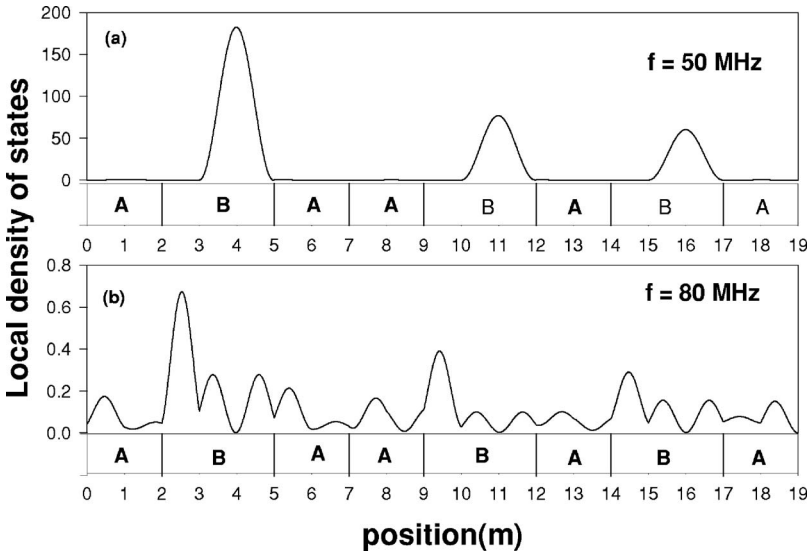

FIG. 4. The theoretical local density of states (in arbitrary units) as a function of the space position for two frequencies (a) 50 and (b) 80 MHz belonging to narrow and large bands of Fig. 2(c), respectively.

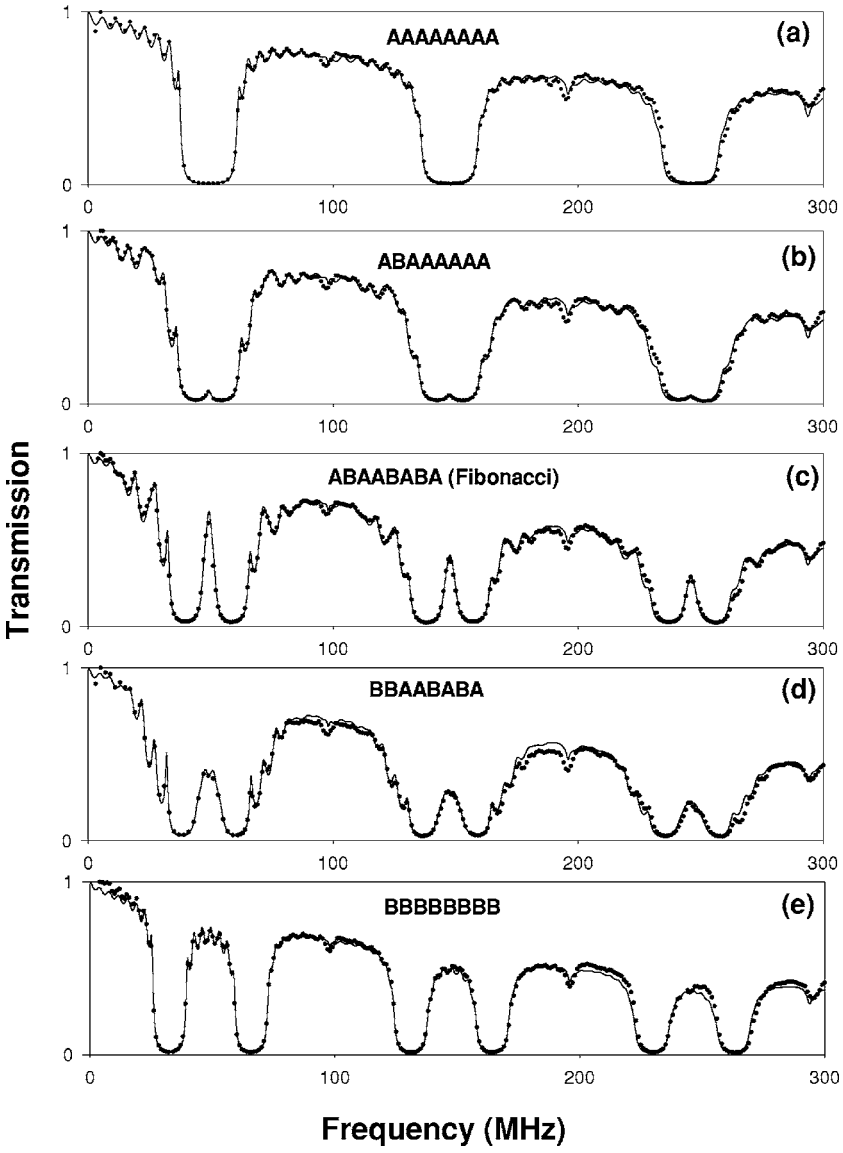

FIG. 5. Theoretical (solid curves) and experimental (dotted curves) variations of the transmission coefficient as a function of the frequency for different structures. (a) The periodic structure made of only *A* blocks. (b), (c), (d) Same as (a) when one, three, and four *A* blocks are substituted by *B* blocks, respectively. (e) Same as (a) but for a periodic structure with only *B* blocks.

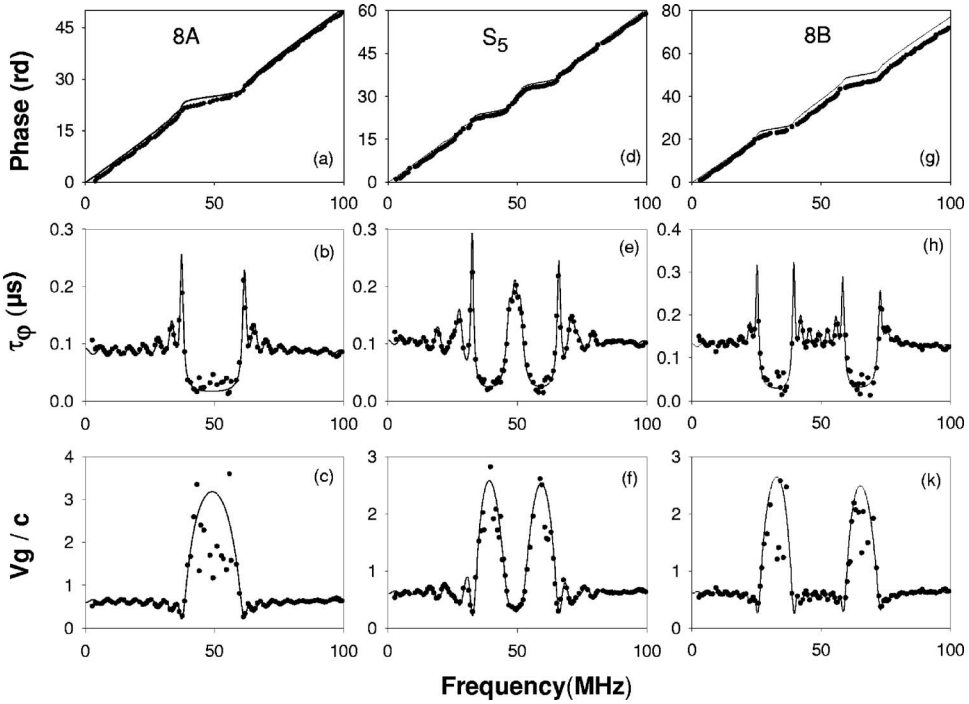

FIG. 6. Theoretical (solid curves) and experimental (dotted curves) phase (a),(d),(g) (top panel), phase time (b),(e),(h) (middle panel), and group velocity (c),(f),(k) (bottom panel) as functions of the frequency for three structures: 8*A* blocks (a)–(c); fifth Fibonacci generation (d)–(f), and 8*B* blocks (g)–(k).

whereas the mode associated with the peak inside the first gap ($f=50$ MHz) shows a strong localization in the *B* blocks and in particular in the segment regions of length $d_B=2$ m [Fig. 4(a)]. The same results are obtained for the other generations. These results clearly show that the modes inside the gaps are localized modes induced by the different segments inside the *B* blocks (see also the discussion of Fig. 7 below). The experimental verification of the nature of the defect modes inside the gaps is presented in Fig. 5. Figure 5(a) presents the transmission coefficient of a periodic structure made of only *A* blocks (8*A*). It can be seen that the band gap structure does not show any features inside the gaps. Now, by substituting one *A* block in the structure by one *B* block [Fig. 5(b)], small defect peaks appear in the middle of the gaps. By increasing the number of *B* blocks substituted in the periodic 8*A* blocks [Figs. 5(c) and 5(d)], other modes detach from the allowed bands and fall inside the gaps, giving rise to new ordered bulk bands when all the *A* blocks are replaced by the *B* blocks [Fig. 5(e)]. These results show that the transmission coefficient of the Fibonacci structure [Fig. 5(c)] composed of binary *A* and *B* blocks may be considered as an intermediate one between those associated with finite periodic systems formed by *A* blocks and by *B* blocks, respectively.

The existence of localized waves in FLSs may be used as a tool to reduce the group velocity of waves in such structures. Indeed, as was argued recently [31], the presence of a single defect in an otherwise periodic system made of two alternating different coaxial cables may reduce considerably the group velocity in a narrow frequency band below the normal propagation speed in the cables. Now, by introducing more than one defect in these structures as in Fibonacci systems, one can obtain a narrow frequency band where the velocity may be slower. These results are illustrated in Figs. 6(a)–6(k) where we have plotted the phase (top panel), the phase time τ_φ (middle panel), as well as the group velocity $v_g=L/\tau_\varphi$ [32] (bottom panel) versus the frequency for three structures: the 8*A* blocks [Figs. 6(a)–6(c)], the fifth Fibonacci generation [Figs. 6(d)–6(f)], and the 8*B* blocks [Figs. 6(g)–6(k)]. *L* is the total length of the finite structure, i.e., the sum of the lengths of the *A* and *B* blocks constituting the structure (see Fig. 4 for the fifth generation). As demonstrated in Sec. II C, symmetric loop structures do not exhibit transmission zeros and hence the phase of the transmission increases monotonically as function of the frequency (top panel of Fig. 6). Consequently, the phase time (middle panel) is equivalent to the density of states in these 1D photonic crystals and the group velocity is equivalent to the inverse of the density of states [32]. In the case of periodic structures [Figs. 6(a)–6(c) and 6(g)–6(k)], an anomalous dispersion occurs inside the gaps and superluminal velocities are expected such that $3c<v_g<3.5c$ [18,25]. This result is not at odds with either causality or the Einstein theory of special relativity, because it results exclusively from interference between the different frequency components of the pulse in an anomalous dispersion region [25]. Inside the passbands, the group velocity is equal to $0.66c$, which is the normal speed of wave propagation in the cables used in these experiments. In the case of a FLS [Figs. 6(d)–6(f)], the structure is disordered, which induces large phase times inside the gaps [Fig. 6(e)] and therefore small group velocities ($v_g\approx 0.3c$) lower than the normal speed in the cables [Fig. 6(f)]. This value is the same as the one found by Munday and Robertson [31] in different coaxial cable structures. The slower group velocity may be explained by the time spent by the photon (trapping time) inside the segments of the *B* blocks (cavities) before its transmission. Another interesting result in Fig. 6 concerns the behavior of the phase time and the group velocity near the band gap edges. Indeed, it is well known that in infinite 1D periodic systems, the density of modes approaches infinity at the band edge and the group velocity becomes very

small. In a finite system, however, the electromagnetic mode density is an oscillating function rather than a monotonic function [Figs. 6(b) and 6(h)]. The enhancement of the phase time (density of states) at the band edges induces a small group velocity ($v_g \approx 0.2c$) [Figs. 6(c) and 6(k)] which has been shown to be of potential interest in application to band edge loss and optical delay lines [33]. In the case of a FLS [Figs. 6(e) and 6(f)] the phase time and the group velocity present similar behaviors at the band edges. However, it was shown recently [8] that the band edge resonances in periodic photonic systems are not localized states since their extension scales linearly with the system size and they do not decay to zero. In contrast, the Fibonacci band edge resonances will decay via a power law due to their critically localized nature.

In order to show the effect of the length of the segments in the B blocks, we have plotted in Fig. 7(b) the theoretical dispersion curves (the frequency f as a function of d_B) for the fifth generation. All other wires in the loops and segments are supposed to be of identical length ($d=1$ m). These frequencies are obtained from the maxima of the phase time (density of states). Figure 7(c) gives an enlargement of Fig. 7(b) in the frequency region below 100 MHz. The open circles correspond to the frequencies obtained from the maxima of the experimental phase time as shown in Fig. 8 for a few values of d_B. The arrows on the frequency axis in Figs. 7(b) and 7(c) indicate the limits of the gaps of the periodic structure ($d_B=1$ m). Figures 7(b) and 7(c) clearly show that the bulk modes are weakly dependent upon d_B, while the defect modes display a strong variation with this length. The localized modes emerge from the bulk band, decrease in frequency when d_B increases, and finally merge into a lower bulk band. The evolution of the three localized branches inside the gap is shown by vertical arrows in Fig. 8. At each frequency inside the gaps of Figs. 7(b) and 7(c), there is a periodic repetition of the localized modes as a function of d_B. This is due to the fact that the functions involving the variable d_B are periodic functions [see Eq. (6)]. Figure 9 presents the same results as Fig. 8 but for the transmission coefficient. One can notice that the three branches inside the gap are not well distinguished one from each other as was the case for the phase time (Fig. 8).

Until now, we have shown that FLSs present similar results as periodic loop structures, but with additional features inside the gaps. These resonances present a certain recursive order which is a characteristic of Fibonacci systems. This property, called the scaling relation [2,3], has been interpreted as a sign for localization of the waves in Fibonacci systems. Kohmoto *et al.* [2] have shown the existence of an invariant I which remains constant at every step of the recursive procedure. In the present system, this expression is given by [29]

$$I = \frac{1}{4}\left(\frac{Z_B}{Z_A} - \frac{Z_A}{Z_B}\right)^2 \sin^2(\omega\sqrt{\varepsilon}d/c)\sin^2[\omega\sqrt{\varepsilon}(d_B - d_A)/c], \tag{15}$$

where $Z_A=25\ \Omega$ and $Z_B=50\ \Omega$ are the impedances of the loops and segments, respectively. Also, it has been demonstrated [2,3] that one can expect scaling around $\delta=\omega\sqrt{\varepsilon}d/c = \omega\sqrt{\varepsilon}(d_A-d_B)/c=(m+1/2)\pi$ where the quasiperiodicity is most effective (m is an integer). This implies that the transmission coefficient should exhibit a self-similar behavior around the central frequency $f_c=(2m+1)49.4$ MHz with $T_{j+3}=T_j$ (the period of the transmission coefficient is three recursion). The scaling behavior of the transmission coefficient is characterized by the scale factor [2,3]

$$F = \sqrt{1+4(1+I)^2} + 2(1+I). \tag{16}$$

For the central frequency $f_c=(2m+1)49.4$ MHz, $I=0.526$ and thus $F=6.4061$. Figures 10(a)–10(d) (left panel) show the transmission coefficient for the generations S_5, S_{11}, S_8, and S_{14} near f_c. Note the scale change of the frequency

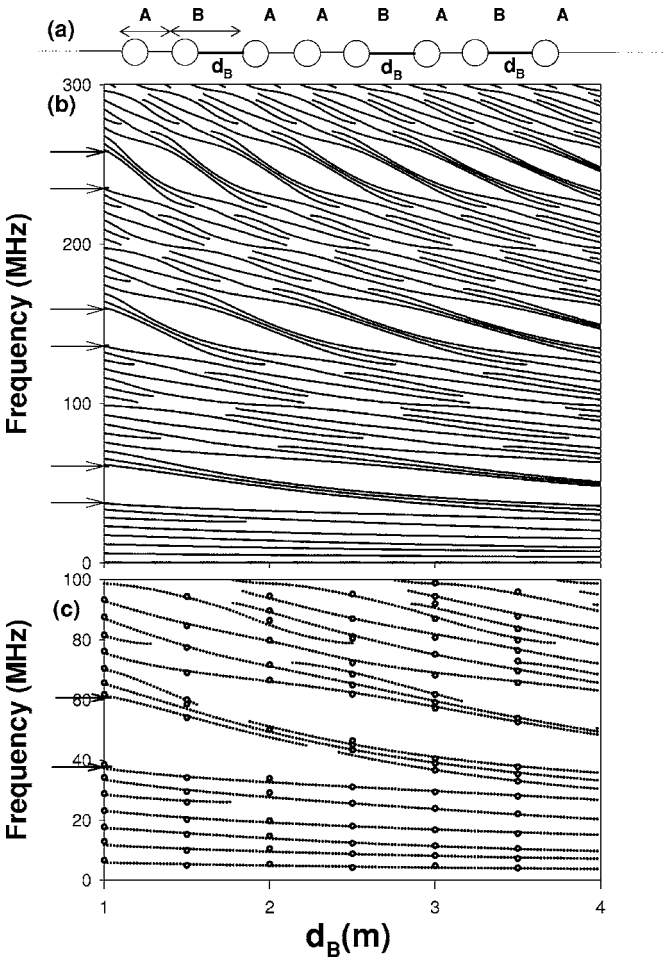

FIG. 7. (a) Schematic illustration of the fifth Fibonacci generation. (b) Projected band structure: frequency as a function of the segment length $d_6=d_B$. The other parameters are the same as in Fig. 2. The dots are obtained from the maxima of the theoretical phase time. (c) The same as (b) but enlarged in the frequency region below 100 MHz. The open circles correspond to the frequencies obtained from the maxima of the experimental phase time. The arrows on the frequency axis show the limits of the gaps of the periodic structure composed of only A blocks ($d_B=1$ m). The modes around the frequencies 10, 100, 200, and 300 MHz correspond to the extended modes, whereas the modes falling inside the gaps represent localized modes.

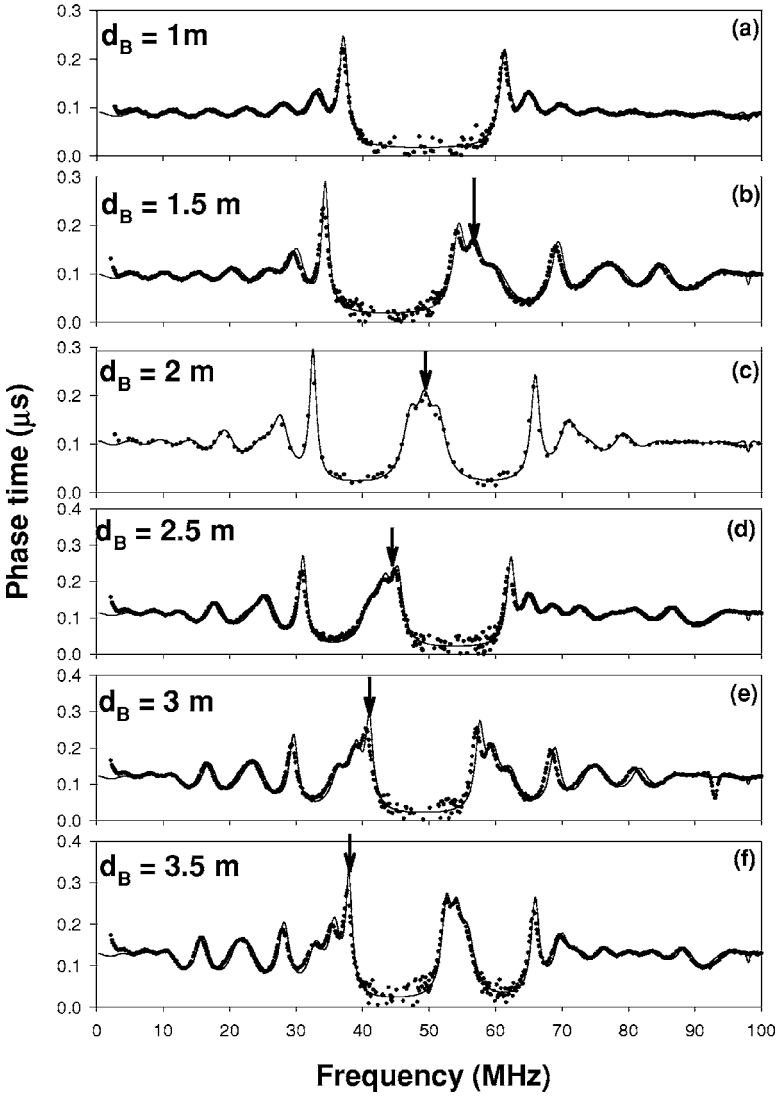

FIG. 8. Theoretical (solid curves) and experimental (dotted curves) variations of the phase time as function of the frequency for a few values of d_B. The vertical arrows indicate the evolution of the positions of the three branches lying inside the first gap.

axis in Figs. 10(a) and 10(b) and Figs. 10(c) and 10(d). Surprisingly, we remark that S_5 (S_8) and S_{11} (S_{14}) resemble each other near f_c with a periodicity of 6 instead of 3 and with a scaling factor $F^2 \approx 41$ instead of F as was found by Kohmoto *et al.* [3]. However, these results are in agreement with those found theoretically by other authors [6,11] on multilayered media by using the transfer matrix method and the complex effective wave number. This discrepancy is due to the fact that Kohmoto *et al.* [3] considered a specific structure in which each block A and B is composed of only one layer and the two substrates are equivalent to the A layer. This was mentioned also by Albuquerque and Cottam [1]. As mentioned above (Fig. 3), the dissipation in the cables limits the experimental study of high Fibonacci generations; therefore we have neglected the absorption in the transmission coefficients of Figs. 10(a)–10(d) so as to give a theoretical verification of the Fibonacci scaling property. This means that this property may be experimentally verified in the case of lossless media [3–7]. In addition, Figs. 10(e)–10(h) (right panel) show that the scaling property is also a characteristic of the transmission phase time and therefore of the group velocity. It is worth noticing here also that as long as we are dealing with symmetric loop structures, the phase of the transmission (not shown) increases monotonically as a function of the frequency.

B. Case of asymmetrical loops in B blocks

In Fig. 7 we have shown the effect of the length of the segments in the B blocks on the dispersion curves, while the lengths of the other wires were kept constant. Now we emphasize the effect of an asymmetric loop in the B block (i.e., $d_4 \neq d_5 \neq 1$ m in Fig. 1) on the dispersion curves, while the lengths of the other wires are kept constant (i.e., $d_1=d_2=d_3=d_6=d=1$ m). In particular, we suppose that the difference between the wires of the loop in the B block $\Delta L=d_4-d_5$ is variable, while the whole length of the loop is kept constant (i.e., $L=d_4+d_5=2$ m). Figure 11 displays the dispersion curves (i.e., the frequency versus ΔL for the fifth generation. The frequencies (dots) are obtained from the maxima of the theoretical phase time calculated in the absence of absorption in the wires. In addition to the resonances lying inside the bulk bands, one can also notice the existence of some resonances that occur at the crossing of two bulk bands. For instance, this happens around $\Delta L=0$ or 2 m at the frequencies $f=100$, 200, and 300 MHz; around $\Delta L=0.66$ and

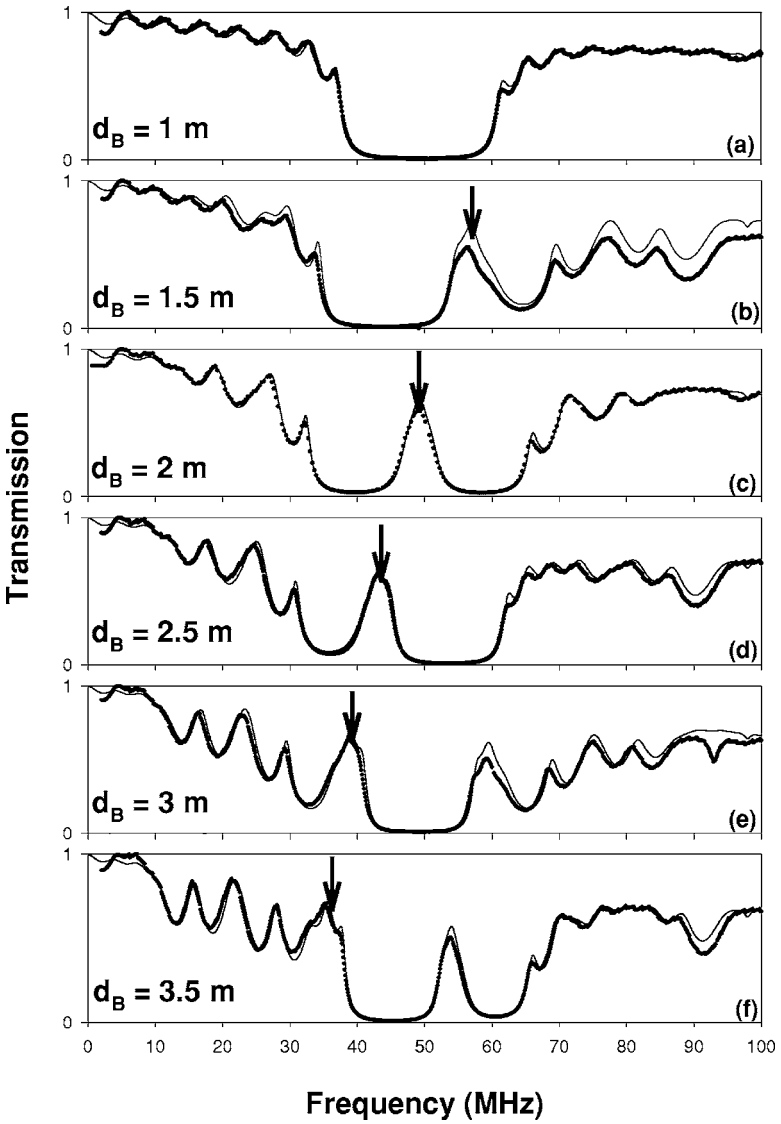

FIG. 9. The same as Fig. 8 but for the transmission coefficient.

1.34 m at $f=300$ MHz; and around $\Delta L=1$ m at $f=200$ MHz. The intensities of the associated peaks in the phase time decay as long as ΔL goes away from the values mentioned above. The dashed horizontal and curved lines correspond to the frequencies at which the transmission through a single asymmetric loop is equal to zero. They are given by [18]

$$\sin(\omega\sqrt{\varepsilon}L/2)=0 \quad \text{and} \quad \cos(\omega\sqrt{\varepsilon}\Delta L/2)=0. \qquad (17)$$

It is worthwhile to notice that almost similar dispersion curves as in Fig. 11 are obtained from the maxima of the transmission coefficient, except for the resonances (discussed above) that occur at the crossings of two bulk bands. This difference is due to the fact that the above resonances in Fig. 11 are located in the close vicinity of zeros of transmission (horizontal dashed lines in Fig. 11), and therefore the power transmission displays a dip instead of a peak. In the particular case where $\Delta L=0$ in Fig. 11 (i.e., $d_4=d_5=d=1$ m, symmetric loop) the FLS becomes a PLS with $8A$ blocks and therefore the gaps around 50, 150, and 250 MHz are introduced by the periodicity of the structure. These stop bands are weakly dependent upon the variation of ΔL. However, when ΔL increases, some additional gaps of a lozenge pattern appear at the crossing of the horizontal and curved dashed lines. These gaps are the consequence of the transmission zeros induced by the asymmetric loops in the B blocks, which play the role of resonators. There are also some narrow minigaps along the dashed curved lines; these gaps are produced by the quasiperiodicity of the structure [18]. For $\Delta L=2$ m (i.e., $d_4=2$ m, $d_5=0$ m), one can show that these loops are equivalent to two dangling side branches of lengths $d_4/2=1$ m. As mentioned in Sec. II C, the transmission phase time in asymmetric loop structures is different from the DOS because of the transmission zeros that induce jumps of π in the phase and thus negative δ functions in the phase time. The discussion of the relation between the DOS and the phase time is very well clarified in Refs. [27,28]. Some experimental verifications of these results are given in Ref. [18] in the case of one asymmetric loop structure. Similar results are found by other authors [34] in two-dimensional photonic crystals of spheres, where it was shown clearly that taking into account the absorption in the system, the DOS increases monotonically whereas the phase

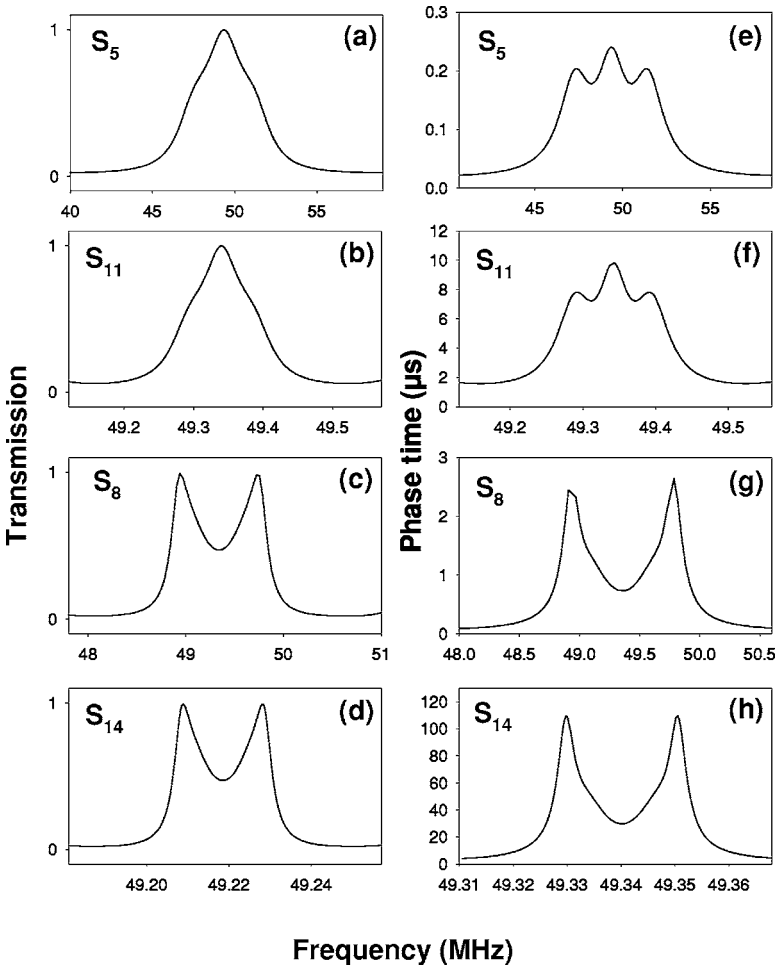

FIG. 10. (a)–(d) (left panel): The transmission coefficient for the generations S_5, S_{11}, S_8, and S_{14} near the central frequency $f_c=49.4$ MHz. (e)–(h) (right panel): Same as (a)–(d) but for the phase time. Note the scale change of the frequency axis in the figures associated to S_5 (S_8) as compared to S_{11} (S_{14}).

shift exhibits a jump at the frequencies of the dips in the transmission coefficient. In the case of periodic and quasiperiodic asymmetric loop structures studied here, we have checked theoretically that the phase increases monotonically and exhibits jumps of π at the frequencies given by Eq. (17). Experimentally, we also observe a monotonic increase of the phase in the allowed bands of the structure; however, in the forbidden bands around the transmission zeros, the transmission is too weak to be detected with enough accuracy and the corresponding phase behaves randomly. That is why we have avoided giving results for the phase time in this case. Nevertheless, in order to give an experimental verification of the band gap structure of Fig. 11, we plotted in Fig. 12 some transmission amplitude spectra for $\Delta L=0$ [Fig. 12(a)], 1 [Fig. 12(b)], and 2 m [Fig. 12(c)]. The vertical dashed lines give the positions of the common gaps for different values of ΔL (Fig. 11). One can notice in Figs. 11 and 12 that contrary to Fig. 7 the variation of ΔL does not induce new modes inside the gaps but rather splits the bulk bands by opening new gaps especially for $\Delta L=1$ [see Fig. 12(b) around $f=100$ and 300 MHz]. It is worth noticing that the dips that appear in the middle of the bands of Figs. 12(a)–12(c) around 100, 200, and 300 MHz are due to the fact that ΔL is slightly different from 0, 1, and 2 because of the small additional lengths due to the T connectors used in the connection of the different cables in the loops and segments. Also, in detail, the modes displayed in Fig. 12 do not exactly correspond to those shown in Fig. 11 because, contrary to the latter case, the results of Fig. 12 take account of the absorption phenomena in the wires. However, both figures display the same information about the positions of the allowed and forbidden bands.

The dispersion curves presented in Fig. 11 are also very dependent upon the length L of the loop. In particular, if L is slightly different from 2 m, very narrow (almost flat) bands appear in the vicinity of $f=100$, 200, and 300 MHz. When L approaches the value of 2 m, these minibands become totally flat and coincide with the dashed horizontal lines (a discussion about these minibands is given in Ref. [35]).

IV. COMPARISON WITH OTHER QUASIPERIODIC STRUCTURES

The Fibonacci sequence is considered as the 1D representation of quasicrystals [36]. Its Fourier transform [37] is a pure point, characteristic of a true quasicrystal-like structure. There exist also other aperiodic structures that involve two different blocks A and B such as the Thue-Morse and double period structures [38]. The Thue-Morse structure is not quasiperiodic but deterministically aperiodic for the singular continuous Fourier spectrum [39]. The Thue-Morse sequence can be defined through the inflation rules $A\rightarrow AB$ and $B\rightarrow BA$. Therefore, the Thue-Morse generations are $S_0=A$, $S_1=AB$, $S_2=ABBA$, $S_3=ABBABAAB$,…, and the numbers of

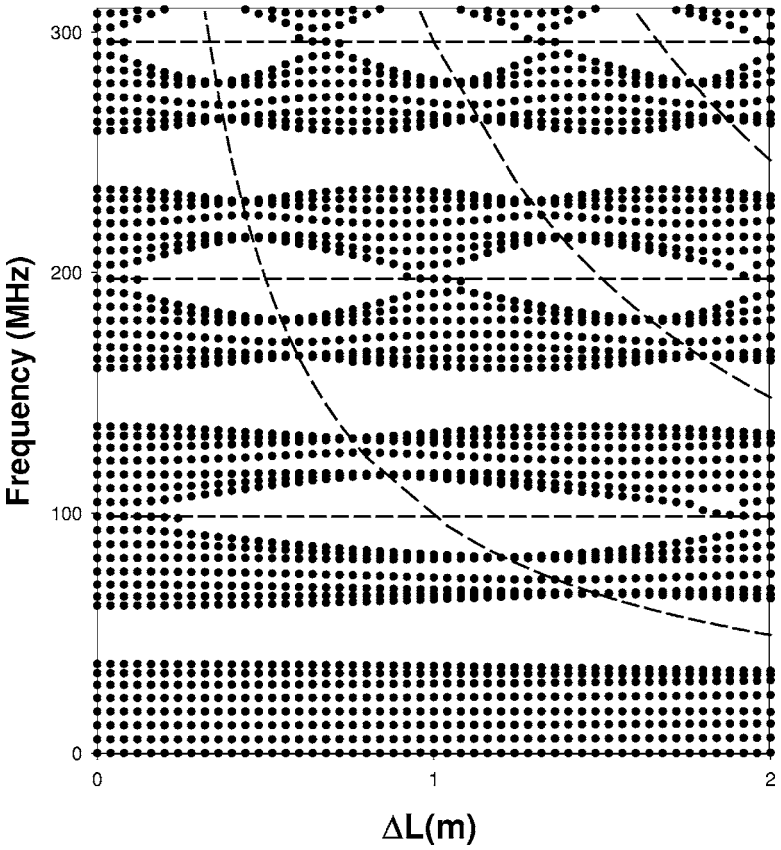

FIG. 11. The projected band structure (frequency as a function of the segment length $\Delta L = d_4 - d_5$) of the fifth Fibonacci generation for $d_1 = d_2 = d_3 = d_6 = 1$ m and $L = d_4 + d_5 = 2$ m. The dashed curves indicate the frequencies at which the transmission through a single asymmetric loop vanishes [Eq. (17)]. The dots are obtained from the maxima of the theoretical phase time.

building blocks A and B in the sequence are equal. The double period sequence can be defined through the inflation rules $A \rightarrow AB$ and $B \rightarrow AA$. Therefore, the double period generations are $S_0 = A$, $S_1 = AB$, $S_2 = ABAA$, $S_3 = ABAAABAB, \ldots$, and the ratio of the number of building blocks A to the number of building blocks B is not constant; it tends to 2 as the number of generations goes to infinity. The final aperiodic structure, called the Rudin-Shapiro structure [40], is more complicated, it involves four different blocks $ABCD$ following the Rudin-Shapiro substitution rules $A \rightarrow AC$, $B \rightarrow DC$, $C \rightarrow AB$, and $D \rightarrow DB$. Therefore, the Rudin-Shapiro generations are $S_0 = A$, $S_1 = AC$, $S_2 = ACAB$, $S_3 = ACABACDC, \ldots$. However, in order to compare the transmission coefficient of this structure with the others cited above, we suppose that the blocks C and D in the Rudin-Shapiro generations are equivalent to A and B, respectively. Let us mention that a numerical comparative study between the transmission amplitudes of Fibonacci, Thue-Morse, and double period structures has been given before for layered media [11]; however, to our knowledge, no comparative study of the phase times of these different structures has been developed.

In what follows, we shall give a theoretical and experimental comparative study of the transmission amplitude and phase time (Fig. 13) between the following structures: (i) a finite sixth Fibonacci generation [Figs. 13(a) and 13(e)] having the structure $ABAABABAABAAB$ involving 13 blocks (8A blocks and 5B blocks); (ii) a finite fifth Thue-Morse generation [Figs. 13(b) and 13(f)] having the structure $ABBABAABBAABABBA$ involving 16 blocks (8A blocks and 8B blocks); (iii) a finite fifth double period generation [Figs. 13(c) and 13(g)] having the structure $ABAAABABABAAABAA$ involving 16 blocks (11A blocks and 5B blocks); (iv) a finite fifth Rudin-Chapiro generation [Figs. 13(d) and 13(h)] having the structure $AAABAABAAAABBBAB$ involving 16 blocks (10A blocks and 6B blocks). All these structures could be considered as a periodic A structure with different B blocks embedded as defects at different positions in this structure. The transmission amplitude and the phase time of these different structures exhibit almost the same behavior inside the frequency regions corresponding to the extended modes. However, these structures present different features inside the first gap around $f = 50$ MHz. In particular, the phase time (right panel of Fig. 13) shows more details about the distribution of the different localized modes induced by the B blocks inside the gap. Indeed, the phase time is less sensitive to the absorption in the cables; that is why the phase time spectra in Fig. 13 give also the density of modes [27] as demonstrated in Sec. II C. An analysis of the local density of states as a function of the space position (not given here) shows that the different modes lying inside the first gap are localized within the segments belonging to the B blocks, whereas the modes lying inside the bulk bands are extended modes within the whole structure.

V. CONCLUSIONS

In this paper, we have given experimental and theoretical evidence for the localization of electromagnetic waves in a

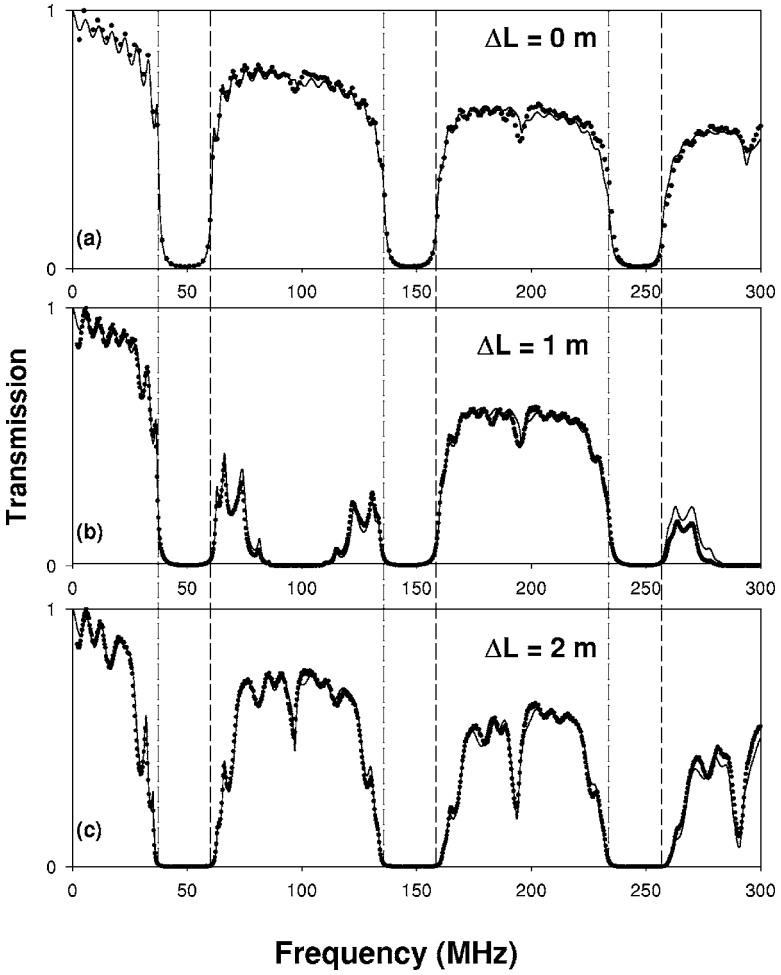

FIG. 12. Theoretical (solid curves) and experimental (dotted curves) variations of the transmission coefficient as a function of the frequency for three values of ΔL in Fig. 11. ΔL=(a) 0 (i.e., $d_4=d_5=1$ m), (b) 1 (i.e., $d_4=1.5$ m and $d_5=0.5$ m), and (c) 2 m (i.e., $d_4=2$ m and $d_5=0$).

FLS made of standard coaxial cables. The symmetric loop structure may play the role of simple alternating layers, which enables us to check easily different localization properties of Fibonacci 1D layeredlike media. However, when the loops are asymmetrical, they play the role of resonators that may introduce transmission zeros and hence new gaps unnoticed in the case of layered media. An analysis of the transmission amplitude and the local density of states clearly shows the origin of the different modes propagating through the FLS. The experimental results are very well fitted by the

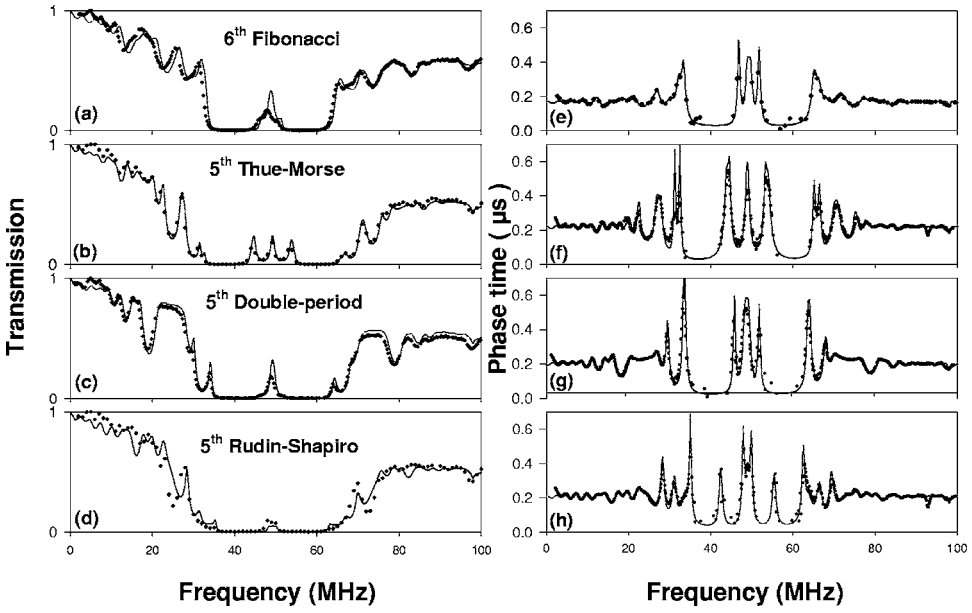

FIG. 13. (a)–(d) (left panel): The transmission coefficient as function of the frequency for the sixth Fibonacci (a), fifth Thue-Morse (b), fifth double period (c), and fifth Rudin-Shapiro (d) generations. (e)–(h) (right panel): Same as (a)–(d) but for the phase time.

1D theoretical model using the Green's function method. An analysis of the phase of the transmission function enables us to deduce several properties of the wave propagation through such structures such as the dispersion curves, the phase times and therefore the density of states, as well as the group velocities. In particular, we have shown that the propagation of electromagnetic waves in FLSs may give rise to a strong normal dispersion inside the gaps and therefore a slow group velocity. Finally, we have given a comparative study of the amplitude and phase time of different quasiperiodic structures such as Fibonacci, Thue-Morse, double period, and Rudin-Shapiro structures. All these structures present similar behaviors in the transmission spectra inside the regions of extended modes; however, they present different localized modes inside the gaps.

ACKNOWLEDGMENTS

E.H.E. gratefully acknowledges the hospitality of the Laboratoire de Dynamique et Structures des Matériaux Moléculaires, Université de Lille 1. This work was supported by "Le Fond Européen de Développement Régional (FEDER), INTERREG III France-Wallonie-Flandre (PREMIO)" and "Le Conseil Régional Nord-Pas de Calais." The work of V.R.V. has been partially supported by the Ministerio de Educación y Ciencia (Spain) through Grant No. MAT2003-04278.

[1] For a review, see, for example, E. L. Albuquerque and M. G. Cottam, Phys. Rep. **376**, 225 (2003).
[2] M. Kohmoto, B. Sutherland, and K. Iguchi, Phys. Rev. Lett. **58**, 2436 (1987).
[3] W. Gellermann, M. Kohmoto, B. Sutherland, and P. C. Taylor, Phys. Rev. Lett. **72**, 633 (1994).
[4] T. Hattori, N. Tsurumachi, S. Kawato, and H. Nakatsuka, Phys. Rev. B **50**, R4220 (1994).
[5] L. Chow and K. H. Guenther, J. Opt. Soc. Am. A **10**, 2231 (1993).
[6] R. Pelster, V. Gasparian, and G. Nimtz, Phys. Rev. E **55**, 7645 (1997).
[7] R. W. Peng, Y. M. Liu, X. Q. Huang, F. Qiu, Mu Wang, A. Hu, S. S. Jiang, D. Feng, L. Z. Ouyang, and J. Zou, Phys. Rev. B **69**, 165109 (2004).
[8] L. Dal Negro, C. J. Oton, Z. Gaburro, L. Pavesi, P. Johnson, A. Lagendijk, R. Righini, M. Colocci, and D. S. Wiersma, Phys. Rev. Lett. **90**, 055501 (2003).
[9] R. W. Peng, M. Wang, A. Hu, S. S. Jiang, G. J. Jin, and D. Feng, Phys. Rev. B **57**, 1544 (1998).
[10] C. Sibilia, I. S. Nefedov, M. Scalora, and M. Bertolotti, J. Opt. Soc. Am. B **15**, 1947 (1998).
[11] M. S. Vasconcelos, E. L. Albuquerque, and A. M. Mariz, J. Phys.: Condens. Matter **10**, 5839 (1998).
[12] X. Huang, Y. Wang, and C. Gong, J. Phys.: Condens. Matter **11**, 7645 (1999).
[13] N. H. Liu, Phys. Rev. B **55**, 3543 (1997).
[14] A. V. Lavrinenko, S. V. Zhukovsky, K. S. Sandomirski, and S. V. Gaponenko, Phys. Rev. E **65**, 036621 (2002).
[15] E. Macia, Phys. Rev. B **63**, 205421 (2001).
[16] D. Lusk, I. Abdulhalim, and F. Placido, Opt. Commun. **198**, 273 (2001).
[17] A. Mir, A. Akjouj, J. O. Vasseur, B. Djafari-Rouhani, N. Fethouhi, E. H. El Boudouti, L. Dobrzynski, and J. Zemmouri, J. Phys.: Condens. Matter **15**, 1593 (2003).
[18] E. H. El Boudouti, N. Fethouhi, A. Akjouj, B. Djafari-Rouhani, A. Mir, J. O. Vasseur, L. Dobrzynski, and J. Zemmouri, J. Appl. Phys. **95**, 1102 (2004).
[19] See, for example, J. D. Joannopoulos, R. D. Meade, and J. N. Winn, *Photonic Crystals* (Princeton University Press, Princeton, NJ, 1995); *Photonic Band Gap and Localization*, edited by C. M. Soukoulis (Plenum, New York, 1993); *Photonic Band Gap Materials*, edited by C. M. Soukoulis (Kluwer, Dordrecht, 1996).
[20] Z. Q. Zhang, C. C. Wong, K. K. Fung, Y. L. Ho, W. L. Chan, S. C. Kan, T. L. Chan, and N. Cheung, Phys. Rev. Lett. **81**, 5540 (1998).
[21] H. Aynaou *et al.*, Physica A **358**, 68 (2005).
[22] L. Dobrzynski, Surf. Sci. Rep. **11**, 139 (1990).
[23] J. O. Vasseur, A. Akjouj, B. Djafari-Rouhani, L. Dobrzynski, and E. H. El Boudouti, Surf. Sci. Rep. **54**, 1 (2004).
[24] G. J. Schneider, S. Hanna, J. L. Davis, and G. H. Watson, J. Appl. Phys. **90**, 2642 (2001).
[25] A. Haché and L. Poirier, Phys. Rev. E **65**, 036608 (2002); J. N. Munday and W. Roberston, Appl. Phys. Lett. **80**, 518 (2002).
[26] M. Buttiker and R. Landauer, Phys. Rev. Lett. **49**, 1739 (1982); E. H. Hange and J. A. Stovneng, Rev. Mod. Phys. **61**, 917 (1989).
[27] M. L. H. Lahlaouti, A. Akjouj, B. Djafari-Rouhani, L. Dobrzynski, M. Hammouchi, E. H. El Boudouti, A. Nougaoui, and B. Kharbouch, Phys. Rev. B **63**, 035312 (2001).
[28] H.-W Lee, Phys. Rev. Lett. **82**, 2358 (1999); T. Taniguchi and M. Buttiker, Phys. Rev. B **60**, 13814 (1999).
[29] G. J. Jin, Z. D. Wang, A. Hu, and S. S. Jiang, J. Phys.: Condens. Matter **8**, 10285 (1996).
[30] B. Djafari-Rouhani, E. H. El Boudouti, A. Akjouj, J. O. Vasseur, and L. Dobrzynski, Prog. Surf. Sci. **74**, 389 (2003).
[31] J. N. Munday and W. M. Roberston, Appl. Phys. Lett. **83**, 1053 (2003).
[32] S. Zhu, N. Liu, H. Zheng, and H. Chen, Opt. Commun. **174**, 139 (2000).
[33] M. Scalora, R. J. Flynn, S. B. Reinhardt, R. L. Fork, M. J. Bloemer, M. D. Tocci, C. M. Bowden, H. S. Ledbetter, J. M. Bendickson, J. P. Dowling, and R. P. Leavitt, Phys. Rev. E **54**, R1078 (1996).
[34] T. Kondo, M. Hangyo, S. Yamaguchi, S. Yano, Y. Segawa, and K. Ohtaka, Phys. Rev. B **66**, 033111 (2002).
[35] A. Akjouj, H. Al-Wahsh, B. Sylla, B. Djafari-Rouhani, and L. Dobrzynski, J. Phys.: Condens. Matter **16**, 37 (2004).
[36] D. Shechtman, I. Blech, D. Gratias, and J. W. Cahn, Phys. Rev. Lett. **53**, 1951 (1984).

[37] E. Bombieri and J. E. Taylor, J. Phys. (Paris), Colloq. **47**, C3–19 (1986).

[38] A. Thue, Skr. Nor. Vidensk.-Akad., [Kl.] 1: Mat.-Naturvidensk. Kl. **7**, 1 (1906); M. Morse, Trans. Am. Math. Soc. **22**, 84 (1921).

[39] Z. Cheng, R. Savit, and R. Merlin, Phys. Rev. B **37**, 4375 (1988).

[40] W. Rudin, Proc. Am. Math. Soc. **10**, 855 (1959); H. S. Shapiro, MS thesis, MIT, Cambridge, MA, 1951 (unpublished).